Asian Journal of Applied Science and Technology (AJAST)
Volume 1, Issue 2, Pages 245-253, March 2017

Automatic Segmentation of the Lumen of the Carotid Artery in Ultrasound B-mode Images

Dr.D.Sasikala[1], S.Ashwathi[2], R.Janani Priya[3], A.Mangaiyarkarasi[4] and S.Kavya[5]

[1]*Head of the Department, Department of ECE, Vivekanandha College of Engineering for Women, Tiruchengode, India. Email: vcewecehod@gmail.com*
[2]*UG Scholar, Department of ECE, Vivekanandha College of Engineering for Women, India. Email: ashwathisaravanan5@gmail.com*
[3]*UG Scholar, Department of ECE, Vivekanandha College of Engineering for Women, India. Email: priyaraj11081995@gmail.com*
[4]*UG Scholar, Department of ECE, Vivekanandha College of Engineering for Women, India. Email: mangaiyarkarasi911@gmail.com*
[5]*UG Scholar, Department of ECE, Vivekanandha College of Engineering for Women, India. Email: kavyasuresh6196@gmail.com*

Article Received: 11 March 2017 *Article Accepted: 21 March 2017* *Article Published: 24 March 2017*

ABSTRACT

A new algorithm is proposed for the segmentation of the lumen and bifurcation boundaries of the carotid artery in B-mode ultrasound images. It uses the hipoechogenic characteristics of the lumen for the identification of the carotid boundaries and the echogenic characteristics for the identification of the bifurcation boundaries. The image to be segmented is processed with the application of an anisotropic diffusion filter for speckle removal and morphologic operators are employed in the detection of the artery. The obtained information is then used in the definition of two initial contours, one corresponding to the lumen and the other to the bifurcation boundaries, for the posterior application of the Chan-vese level set segmentation model. A set of longitudinal B-mode images of the common carotid artery (CCA) was acquired with a GE Healthcare Vivid-e ultrasound system (GE Healthcare, United Kingdom). All the acquired images include a part of the CCA and of the bifurcation that separates the CCA into the internal and external carotid arteries. In order to achieve the uppermost robustness in the imaging acquisition process, i.e., images with high contrast and low speckle noise, the scanner was adjusted differently for each acquisition and according to the medical exam. The obtained results prove that we were able to successfully apply a carotid segmentation technique based on cervical ultrasonography. The main advantage of the new segmentation method relies on the automatic identification of the carotid lumen, overcoming the limitations of the traditional methods.

Keywords: New algorithm, Ultrasound images, Common carotid artery (CCA), Segmentation and B-mode.

1. INTRODUCTION

The common carotid artery (CCA) is the one that supplies the human head, specifically the front part of the brain, and neck, with oxygenated blood. Like other arteries, which purpose relies in the supply of blood from the heart, as the coronary arteries, the carotid is also in risk of developing several diseases, like atherosclerosis, known as the "hardening of the artery", after the accumulation of fatty substances, i.e. lipoproteins, in the artery walls. This accumulation is known as "plaque" and decreases the blood supply. The carotid artery, specifically at the bifurcation, which separates the external (ECA) and internal (ICA) carotid arteries, is one very susceptible to atherosclerosis, mainly because of the high hemodynamic forces that can be found at the bifurcation and branching structures.

Non-invasive ultrasound imaging has been widely used in the diagnosis of cardiovascular diseases, in particular concerning the atherosclerosis with the evaluation of the intima-media thickness (IMT), assessing the distance between the lumen of the carotid artery, that is, where the blood flows, and the inner boundary of the adventitia. This measure, and consequent diagnosis of atherosclerosis among other cardiovascular diseases, is performed with the aid of B-mode ultrasound imaging, requiring the detection of not only the lumen boundaries but as well as of both the near and far adventitia. Therefore, it has been and continues to be a great interest in the efficient automatic segmentation of the adventitia and lumen boundaries in B-mode ultrasound images of the carotid artery. According to Halenka (1999), in this type of images the carotid adventitia appears as two almost parallel lines, known due to their echogenic characteristics, separated in the middle by a hipoechogenic space, known as the "double line" pattern (Halenka, 1999).

Ultrasound B-mode imaging has been the most widely used technique in image-based cardiovascular diagnosis due to the fact of the carotid being a superficial artery and quite suitable for this type of imaging. However, B-mode images present difficulties, specifically in the segmentation of the structures involved, due to several imaging characteristics like low contrast, speckle noise, echo shadows and artifacts, which lead to images of very poor quality that usually require the interaction of an expert. Some works that use several statistical distributions can be found in the literature to cope the granular speckle noise in non-compressed ultrasound signals, like, for example, the Rayleigh distribution (Wagner et al., 1983; Sarti et al., 2004) and K-distribution (V.Dutt et al., 1994; R.C. Molthen et al., 1993). However, most of the signals that are actually used in ultrasound imaging and medical practice are log-compressed signals, which are therefore, unsuitable for the application of statistical distributions because of the reduced intensity range that is characteristic of this type of signal. In 2006, Noble (Noble et al., 2006) described the success of texture segmentation techniques in the classification of breast masses and liver and kidney tissues in ultrasound images. However, the segmentation of the carotid artery tends to be more difficult due to the extremely low degree of discrimination of this structure in the usual ultrasound B-mode images.

Ultrasound imaging represents an extreme and complex challenge to the automatic segmentation algorithms, as for the reasons described earlier, as for the amount of boundary edges that may be missing in the image, leading to gaps in the vessel boundaries. Additionally, as different anatomical regions of the carotid can be acquired in ultrasound B-mode imaging, and also due to the variability of its shape among subjects, a model based segmentation is not appropriate. Despite these difficulties, there has been an increasing interest in ultrasound imaging-based medical diagnosis as consequence of the technological advances verified in this methodology, not only in terms of image quality, but also because of its non-invasive characteristics and low cost (Rui Rocha et al., 2011).

The desired segmentation can be addressed by two main steps: i) the definition or estimation of a region of interest (ROI) of the carotid artery in the B-mode ultrasound image and ii) the delineation of the boundaries of the structure desired, which depends on the ROI defined and can be the artery lumen, intima or adventitia. For this reason, we may consider that the two steps are not independent from each other, since the correct delineation of the artery wall in the segmentation algorithm is strictly connected to the right definition of the ROI.

In this paper, a method is proposed for the automatic identification of the lumen region and consequent segmentation of the lumen boundaries in longitudinal B-mode images of the CCA. The method searches for hipoechogenic structures in the input image, and the lumen region of the CCA is identified based on mean and standard deviation calculations concerning the image intensity. Afterwards, the lumen and bifurcation boundaries of the carotid artery are identified through the application of a geometrical model, in particular, using the Chan-Vese level set model. The method is robust to speckle noise, does not require human interaction and can adjust well the segmentation contours to the lumen boundaries represented in the input images.

2. EXISTING METHOD

Carotid Artery Segmentation Using Graph Cut Algorithm

This paper proposes a scheme for segmenting carotid artery ultrasound images using graph cuts segmentation approach. Region homogeneity constraints, edge information and domain specific information are incorporated during the segmentation process. A graph with two terminals (source and sink) is formed by considering every pixel as a graph node. Each pair of neighbouring nodes is connected by a weighted edge, where the weight is set to a value proportional to the intensity of the gradient along them. Moreover, each graph node is connected to the source and the sink terminals with weights that reflect the confidence that the corresponding pixel belongs to the object and the background, respectively. The segmentation problem is solved by finding the minimum cut through the constructed graph. Experiments using a dataset comprised of 40 B-mode carotid artery ultrasound images demonstrates good segmentation results with (on average) 0.677 overlap with the gold standard images, 0.690 precision, and 0.983 sensitivity.

Image segmentation can be formulated as an energy minimization problem. The minimization of such an energy function corresponds to partitioning image pixels into object and background segments. Several optimization techniques can be used to minimize such energy function. The success of the graph cuts based segmentation schemes can be attributed to the combination of both region and edge information during the segmentation process. The region information forces the homogeneity of the segmented area. Meanwhile, the incorporation of the edge information prevents the leak (i.e. overgrowth of the segmented region) that generally appears in most region-based segmentation schemes.

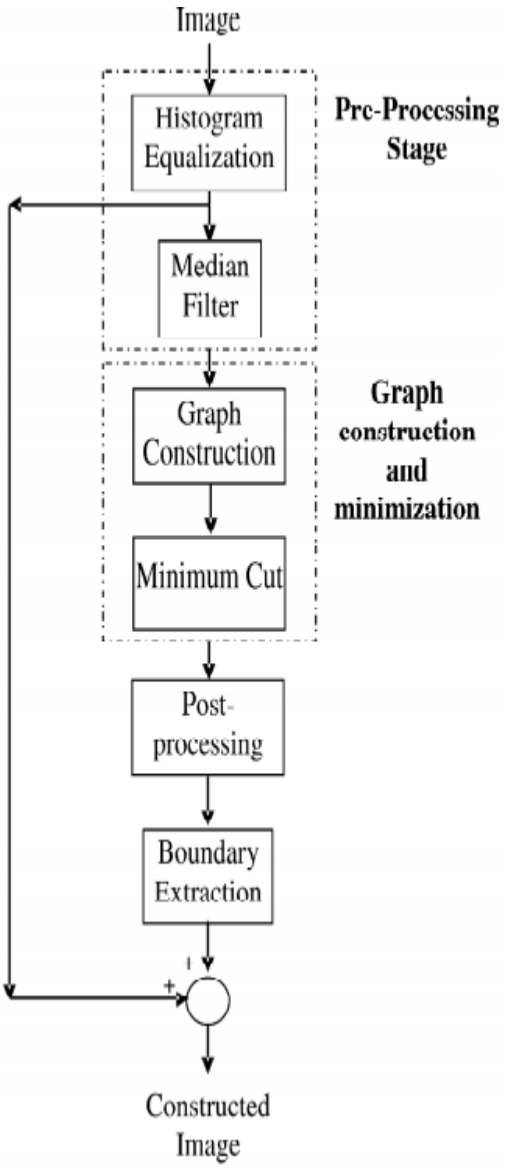

Pre-processing Stage

Ultrasound images suffer from several drawbacks. One of these drawbacks is that ultrasound images have relatively low contrast. Another severe problem is the presence of random speckle noises, caused by the interference of the reflected ultrasound waves. These factors severely degrade any automated processing and analysis of the images. Hence, it is crucial to enhance the image quality prior to any further processing. In this stage we try to overcome these problems by performing two pre-processing steps. The first is a

histogram equalization step to increase the dynamic range of the image gray levels. In the second step, the histogram equalized image is filtered using a median filter to reduce the amount of the speckle noise in the image. It was empirically found that a 3×3 median filter is suitable for the removal of most of the speckle noise without affecting the quality of the edges in the image.

Graph Construction and Minimum Cut Finding

In this stage, the pre-processed image is segmented using graph cuts-based segmentation approach, described in Section 2. First, a two terminal weighted graph is constructed for the image under consideration. Second, the weights of terminal-links and neighbour-links are set. Finally, the minimum cut through the graph is generated using Boykov et al. algorithm [35]. Graph nodes that remain connected to the source node represent object pixels, whereas nodes connected to the sink node represent background pixels.

The weight of a terminal-link is set to a value that reflects our confidence that the given pixel belongs to either the object or the background. Due to the nature of the carotid artery ultrasound images, the area inside the artery (which is the object of interest) is darker than the rest of the image. Hence, pixels with intensities less than a certain object threshold µobject are connected by terminal links to both source and sink nodes with weights equal to one and zero, respectively. Meanwhile, pixels with intensities greater than a background threshold µbackground are connected by terminal links to the source and sink nodes with weights equal to zero and one, respectively. This way, the domain specific information is considered. All other nodes are connected to source and sink nodes with links that have certain weights. A terminal link weight (for a given node) is calculated by a non-negative decreasing function of the absolute differences between the node's intensity and the object and the background thresholds, µobject, µbackground, respectively (this represents a region homogeneity constraint). In the proposed scheme we used an exponential function to calculate the terminal-link weights, as described in Equation (1) and Equation (2).

$$W_{P,Source} = \begin{cases} 1 & if \ I_P \le \mu_{object} \\ 0 & if \ I_P \ge \mu_{background} \\ e^{-\left(\frac{I_P - \mu_{object}}{\alpha}\right)^2} & otherwise \end{cases} \quad (1)$$

and,

$$W_{P,Sink} = \begin{cases} 0 & if \ I_P \le \mu_{object} \\ 1 & if \ I_P \ge \mu_{background} \\ e^{-\left(\frac{I_P - \mu_{background}}{\alpha}\right)^2} & otherwise \end{cases} \quad (2)$$

Where, WP,Source and WP,Sink are the weights of the terminal link connecting node P to the source and the sink nodes, respectively. I P is the intensity of pixel P. µobject and µbackground are the object and the background thresholds, respectively. It is a regulating term, used to control the rate of decay for the exponential weight function. This regulating term allows the weight function to cope up with the fuzzy (or defused) boundaries of the objects within the ultrasound images. We empirically set µobject and µbackground to 10% of the lower and higher intensity ranges, respectively. Whereas a is set to 2% of the total intensity range. Hence, for 8-bit images, we set µobject to 25, µbackground to 230 and a to 5. Note that, in ultrasound images, the object of interest appears darker than the background.

We used the 8-connectivity neighbourhood system, as shown in Figure 3, to assign the neighbour-link weights. These weights are set based on local gradients according to Equation (3),

$$W_{P,Q} = e^{-\left(\frac{I_P - I_Q}{\sigma}\right)^2},$$

Where, WP,Q is the weight of the neighbour-link connecting nodes P and Q, IP and I Q are the intensities of pixels P and Q, respectively, and s is the standard deviation of the gradient magnitude through the image. Note that neighbour-link weights represent the edge information. By finding the minimum cut through the graph edges, a binary image, which separates the object from the background, is formed. The extracted object contains the area inside the carotid artery and some dark objects that usually exist in a given ultrasound image. The user can specify a seed point within the artery to extract the artery wall and neglect all other objects which are outside the region of interest.

Post-processing Stage

The objective of this stage is to smooth the edges of the segmented area and to fill any gaps or holes that may present due to the presence of noise in ultrasound images. Hence, we used a morphological opening operation [36] [37] with a rounded square structuring element of size W. The size of the structuring element can be adjusted, based on the maximum gap size in the segmented area, according to Equation (4),

$$W = (h \times 2) + 1,$$

Where, W is the size of the structuring element and h is the maximum gap size that exists in the segmented image. We empirically found that generally, the maximum gap size does not exceed two pixels. Hence we used a 5×5 structuring element.

Boundary Extraction Stage

The objective of this stage is to extract the boundaries of the segmented regions. Various edge detection schemes can be used for this purpose [36]. In our system, we use a morphological-based contour extraction mechanism [36], [37]. First, the image produced by the previous stage is morphologically eroded using a 3×3 rounded square

structuring element. Then, the eroded image is subtracted from the non-eroded image to obtain the boundary of the segmented region, which represents the artery wall. This operation can be described by Equation (5),

$$\text{Boundary}(A) = A - (A \theta B),$$

Where, A is the post-processed image and B is the structuring element. Finally, the extracted contour is superimposed on the histogram equalized image to produce the final output of the proposed scheme.

3. PROPOSED METHOD

Block diagram

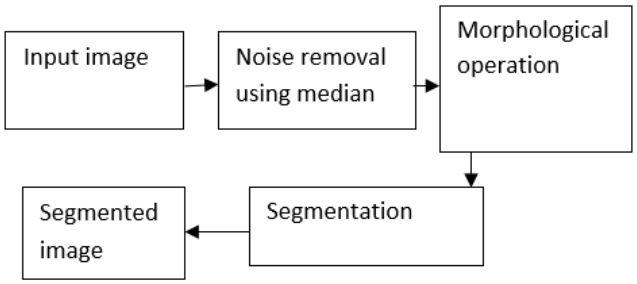

Noise removal using median filter

The median filter is also the simpler technique and it removes the speckle noise from an image and also removes pulse or spike noise. The Median Filter is performed by taking the magnitude of all of the vectors within a mask and sorting the magnitudes. The pixel with the median magnitude is then used to replace the pixel studied. The Operation of median filter can be expressed as:

$$f(x,y) = \text{median}_{(s,t)\in Sxy}\{g(s,t)\}$$

Where Sxy represents the set of coordinates in a rectangular sub image window, centered at point (x,y), and median represents the median value of the window.

Morphological operation for background elimination

Methods of mathematical morphology act based on the structural properties of objects. These methods use mathematical principles and relationships between categories to extract the components of an image, which are useful in describing the shape of zones. Morphological operators are nonlinear, and two sets of data are their input. The first set contains the original image and the second one describes the structural element (mask). The original image is binary or in gray level and the mask is a matrix containing zero and one values. It is after applying the final image to the morphological operators that a new value for each pixel is obtained through sliding the mask on the original image. Value 1 in each mask indicates effectiveness and value 0 indicates ineffectiveness in the final image. Different formats can be selected to form a mask. Figure 1 shows a disk-shaped mask with radius of 4 (9 * 9 matrix).

Morphological Operators

If A (x, y) and B (u, v) describe the gray-level image matrix and the structural element matrix respectively, erosion and dilation operators are defined as (1) and (2):

$$A\Theta B = \min_{u,v}\{A(x+u, y+v) - B(u,v)\}$$

$$A \oplus B = \max_{u,v}\{A(x+u, y+v) - B(u,v)\}$$

The erosion operator reduces the size of objects. This operator increases the size of holes in an image and removes very small details of that image. Removing bright areas under the mask makes the final image looks darker than the original image. The dilation operator acts in reverse; in other words, it increases and decreases the size of objects and holes in the image respectively. The opening operator is equivalent to the application of the erosion and dilation operations on the same image respectively (Equation (3)) while the closing operator acts in reverse (Equation (4)):

$$A \circ B = (A\Theta B) \oplus B$$

$$A \cdot B = (A \oplus B)\Theta B$$

The opening operator removes weak connections between objects and small details while the closing operator removes small holes and fills cracks.

Selecting a Proper Mask

Selecting a mask in proper shape and size to take morphological actions has a key role in achieving desired results and reducing calculation time. In general, the shape and size of a mask are arbitrarily selected; however, the selected mask should be in appropriate shape and size for various diagnosis purposes. Disk-shaped masks (Figure 1) are more commonly used for medical images than other masks. As stated before, since disk-shaped masks are independent of changes in rotation, they are chosen for medical images. Since big or small masks strengthen or weaken various parts of an image, it is impossible to gather detailed information on the contrast of different images using only one structural element. This is why one mask in a particular shape and size may not appropriate for other applications [9]. In the proposed method, the change in shape and size of the mask continues until an appropriate result obtained. It should be mentioned that past experiences have key roles in selecting proper masks to take morphological actions.

Top-Hat Transforms

These transforms are used to enhance the contrast of images through morphological methods and are in two general types: Top-Hat transform is obtained by subtracting the opening of the original image from the image itself (Equation (5)) and Bottom-Hat transform is obtained through subtracting the original image from its closing (Equation (6))

$$\text{Top-Hat}(A) = ATH = A - (A \circ B) \quad (5)$$

$$A_q = A + ATH - ABH \quad (6)$$

Top-Hat and Bottom-Hat transforms are generally known as Open Top-Hat or White Top-Hat and Close Top-Hat or Black Top-Hat respectively. In many papers, Top-Hat is used to refer to both kinds of hat transforms. These transforms are named Top-Hat after Cylinder Hat.

Segmentation using Active disc optimization

Active contours, also called snakes, are used extensively in computer vision and image processing applications, particularly to locate object boundaries .Active contours, or snakes, are curves defined within an image domain that can move under the influence of internal forces coming from within the curve itself and external forces computed from the image data. The essential idea is to evolve a curve or a surface under constraints from image forces so that it is attracted to features of interest in an intensity image. Snakes are widely used in many applications, including edge detection, shape modelling, segmentation, and motion tracking.

Boundary based level set methods presented thus far provide efficient and stable algorithms to detect contours in a given image. The presented methods handle changes in topology and provide robust stopping terms to detect the goal contours. However, structures such as interior of objects, e.g. interior of discs are not segmented. Because of level set formulation the final contours are always closed contours. In addition, in images where the objects object boundaries are noisy and blurry these methods face some difficulties. Some recent works in active contours consider these issues. There are some objects whose boundaries are not well defined through the gradient. For example, smeared boundaries and boundaries of large objects defined by grouping smaller ones.

Step1: Identification of the image area and consequent reduction of the image size

As a first step, we intend to reduce the image area, eliminating any possibility of detecting unwanted features that do not belong to the ultrasound data to be analyzed. This procedure also reduces the time required in the posterior steps of image processing and segmentation. The reduction of the image data consists in the definition of a rectangular area involving the carotid artery (Golemati et al., 2007). With this goal in mind, four points are identified by the following procedure: (1) Morphological opening of the original image, using a circular element to remove unwanted objects such as characters; (2) Image binarization, as such, the areas outside the region of the ultrasound data to be analyzed are discarded; (3) Finally, the four points that correspond to the first and last nonzero lines and columns of the binary image are identified. These points are the vertices of the rectangular area in which all the further tasks of image processing and segmentation are performed.

Lumen region identification

This procedure is based on the study performed by Liboni et al. (2007) to develop a computer-based tracing of the carotid artery. According to these authors, the carotid characteristics in an ultrasound image can be addressed using a model of variable intensity distribution over the carotid regions. It is precisely this idea that is used here for the automatic identification of the lumen of the carotid artery. Pixels belonging to the lumen region of the carotid artery are those characterized by both low mean and standard deviation intensity values (Liboni et al. (2007)). In order to proceed with this identification, 2D histograms are built: For each pixel of the image to be analyzed, it is calculated within a neighborhood the mean and standard deviation intensity values; both values are then normalized and grouped into a set of classes.

A row-wise intensity distribution is built for each column of the ultrasound image region to be analyzed so the pixels corresponding to the carotid artery can be identified. However, the image data must be previously processed for speckle noise removal and attenuating the high intensity noisy points in the intensity distribution; in this task, a Gaussian low-pass filter is used. As mentioned previously, pixels belonging to the lumen region of the carotid artery are those characterized by their low mean and standard deviation intensity values. Having this into consideration, those pixels are identified in the intensity distributions built as being those related to the minimum values presented, which are frequently between the local maximums corresponding to the near and far adventitia layers, or corresponding to the walls of the ICA and ECA, or in the interval between these two borders, if it is considered a column of the image containing pixels belonging to the carotid bifurcation. Based on Liboni et al. (2007) approach, the identification process starts from the bottom of the image to be analyzed, i.e. from the highest row index, and moves upwards along the rows in order to correctly identify the first pixel of the first maxima which as possibly corresponds to the far adventitia of the carotid that is usually associated to the brightest structure of the ultrasound image of the carotid artery. Having this first pixel estimated as possibly belonging to the far adventitia, the method continues the lumen identification moving upwards and searching for a pixel possible belonging to the lumen region. Taking into account the row of the pixel that corresponds to the far adventitia, the pixel possibly belonging to the lumen is the first minima point after the far adventitia pixel. Also, its neighborhood mean and standard deviation intensity values must match the chosen criteria for the 2D histogram.

Lumen edges identification

Having obtained the correct identification of a group of pixels belonging to the lumen of the carotid artery presented in the input image, the definition of a suitable mask for a level set-based segmentation is possible. However, some processing techniques must be applied to the image to be segmented in order to assure the robustness of the segmentation process. Hence, an anisotropic diffusion filter is applied in order to attenuate the high amount of speckle noise that is commonly present; the filter proposed in (Perona and Malik, 1990) with a 2D network structure of 8 neighboring nodes for diffusion conduction was chosen to accomplish such smoothing. Then, it is applied a morphological closing

operator in order to merge small "channels" and "openings". Thirdly, a threshold based on the value defined based on the image histogram is performed. This threshold results in a binary image on which is applied the Sobel gradient operator in order to identify the edge points. The binary image obtained with the application of the Sobel operator combined with the information relevant to the pixels that belong to the lumen region of the carotid allow the identification of the edges correspondent to the superior and inferior wall of the lumen of the carotid artery. Figure 2E shows that combination; in this figure, it can be observed the pixels of the lumen candidate string with the highest column value (located in the rightest part of the image), which can be searched in the binary image resulted from the Sobel operator, the pixels above and below (at the same column) with value 1 (one). Having the row and column of these two pixels found, one belonging to the superior lumen edge and the other to the inferior one, it is possible to trace the remainder of the edges in the Sobel binary image and store the coordinates of each pixel in a string. As such, two strings are built having the coordinates of each pixel belonging to the superior and inferior lumen edges. Posteriorly, a new string is defined containing the pixels belonging to the bifurcation edge in the binary image, knowing that the bifurcation is located between the superior and inferior walls of the carotid. Finally, two masks are defined for posterior application of the geometrical model of Chan-Vese for the segmentation of both bifurcation and common carotid artery walls, as shown in Figure 4. These masks are created with the information of the superior and inferior walls of the carotid artery, as well as its bifurcation, by filling its interior with pixels of value 1 (one), and the outside with pixels of value 0 (zero), creating a binary image.

Segmentation of the lumen and bifurcation boundaries of the carotid artery using the Active disc method

It is a powerful segmentation method that can be used to detect the lumen boundaries of the carotid artery using the two masks built in the previous step as initial contours. This segmentation approach is well known for its high flexibility and accuracy as is a region-based model independent of gradient information. This independence makes the segmentation robust to cases in which gaps exist in the boundaries of the carotid as usually occur. The segmentation both of the lumen and bifurcation boundaries of the carotid artery is based on the work developed by Lankton and Tannenbaum (2008) that defined a local-based framework according to the active contour moves according to an internal energy defined in the Chan-Vese approach using a constant intensity model. The framework starts with the input of an initial contour, here, one of the masks built in the previous step, and the definition of a signed distance function defined as:

$$\phi = E_d(m) - E_d(1-m) + \left(m - \left(\frac{1}{2}\right)\right),$$

Where m represents the initial contour and is the Euclidean distance transform of the considered binary image, assigning for each pixel, the distance between them and the nearest nonzero value. Let C represent a closed contour, as the zero level of, i.e., { ( ) }, where its interior is expressed respectively as:

$$H\,\phi(x) = \begin{cases} 1 & ,\phi(x) < -\epsilon \\ 0 & ,\phi(x) > \epsilon \\ \frac{1}{2}\left\{1 + \frac{\phi}{\epsilon} + \frac{1}{\pi}\sin\left(\frac{\pi\phi(x)}{\epsilon}\right)\right\} & ,otherwise \end{cases},$$

Having and as independent variables representing the coordinates of a pixel in the domain Ω of an image, the following equation represents a function defining a region of interest (ROI) of radius, with value 1 (one) inside and 0 (zero) outside:

$$B(x,y) = \begin{cases} 1, & \|x-y\| < r \\ 0, & otherwise \end{cases}.$$

With eq. (4), the energy functional can be defined as:

$$E(\phi) = \int_{\Omega_x} \delta\,\phi(x) \int_{\Omega_y} B(x,y).F\big(I(y),\phi(y)\big)\,dy\,dx,$$

Where ( ) prevents the development of new contours by ensuring that C does not undergo sudden changes in its geometry. On the other hand, it will allow certain parts of the contour C to separate or combine within each other. Each pixel in this term is masked to ( ) ensuring that only the local information surrounding C will be used.

The smoothness of the contour C is assured through the application of a regularization term that penalizes its arc length. The weight of this penalty is controlled by the parameter in the new equation of the energy functional:

$$E(\phi) = \int_{\Omega_x} \delta\,\phi(x) \int_{\Omega_y} B(x,y).F\big(I(y),\phi(y)\big)\,dy\,dx + \lambda \int_{\Omega_x} \delta\,\phi(x)\|\nabla\,\phi(x)\|\,dx.$$

Lanktom and Tannenbaum (Lanktom and Tannenbaum, 2008) proposed the introduction of specific energies into the generic framework described previously, including the Chan-Vese energy that is expressed as:

$$E_{CV} = \int_{\Omega_y} H\,\phi(y)(I(y)-u)^2 + \big(1 - H\,\phi(y)\big)(I(y)-v)^2\,dy,$$

$$u = \frac{\int_{\Omega_y} H\,\phi(y).I(y)\,dy}{\int_{\Omega_y} H\,\phi(y)\,dy},$$

$$v = \frac{\int_{\Omega_y} (1-H\,\phi(y)).I(y)\,dy}{\int_{\Omega_y} (1-H\,\phi(y))\,dy}.$$

The corresponding Chan-Vese internal energy function is based on the local mean intensities and, instead of and:

$$F_{CV} = H\,\phi(y)(I(y)-u_x)^2 + \big(1 - H\,\phi(y)\big)(I(y)-v_x)^2,$$

$$u_x = \frac{\int_{\Omega_y} B(x,y)H\,\phi(y).I(y)\,dy}{\int_{\Omega_y} B(x,y)H\,\phi(y)\,dy},$$

$$v_x = \frac{\int_{\Omega_y} B(x,y)(1-H\,\phi(y)).I(y)\,dy}{\int_{\Omega_v} B(x,y)(1-H\,\phi(y))\,dy}.$$

$$\Leftrightarrow \frac{\partial \phi}{\partial t}(x) = \rho\,\phi(x)\int_{\Omega_\lambda} B(x',\lambda)\,\rho\,\phi(\lambda)\left((I(\lambda)-\mu^x)_2 - (I(\lambda)-\mu^x)_1\right)d\lambda + \gamma\,\rho\,\phi(x)\,\mathrm{div}\left(\frac{\nabla\phi(x)}{|\nabla\phi(x)|}\right)\cdot$$

$$\frac{\partial \phi}{\partial t}(x) = \rho\,\phi(x)\int_{\Omega_\lambda} B(x',\lambda)\,\Delta^{\phi(\lambda)}\mathrm{h}\left(I(\lambda),\phi(\lambda)\right)d\lambda + \gamma\,\rho\,\phi(x)\,\mathrm{div}\left(\frac{\nabla\phi(x)}{|\nabla\phi(x)|}\right) \Leftrightarrow$$

$$\Delta^{\phi(\lambda)}\mathrm{h} = \rho\,\phi(\lambda)\left((I(\lambda)-\mu^x)_2 - (I(\lambda)-\mu^x)_1\right)' \qquad (1$$

The Chan-Vese energy function finds its minimum when the interior and exterior of the curve are closer to the global mean intensities and , while in the localized version, the minimum is obtained when they are closer to the local mean intensities and .

For the segmentation of the bifurcation boundaries, the mask illustrated in Figure 3g is chosen as the initial contour. The level set for the segmentation of these boundaries must be flexible in order to reach the limit of the bifurcation walls. On the other hand, for the segmentation of the lumen boundaries, the mask illustrated in Figure 3f is defined and the development contour C has to be properly controlled and somehow attenuated in order to prevent its development towards other structures near the carotid artery. The circular ROI ( ) has also to be chosen narrow in order to prevent larger intensity variations during the contour C development along the Chan-Vese energy minimization process.

Contour smoothness

Finally, the obtained contours must be smoothed: Firstly, through a cubic spline interpolation and secondly, by projecting all the resulting points of the contour towards a local regression line. Once again, a ROI is defined for each point of the contour, regarding the number of points in the neighborhood that contribute for the computation of the local regression line. In this process, for each pixel we defined an 8-connected-neighborhood for its computation.

4. RESULTS

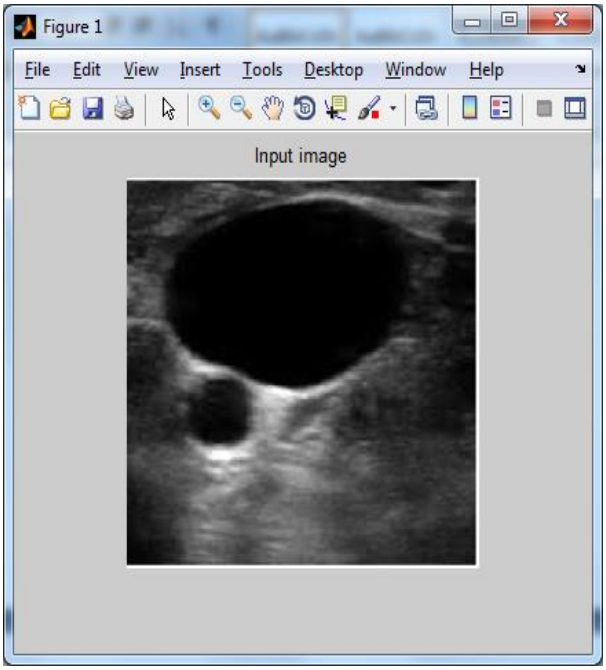

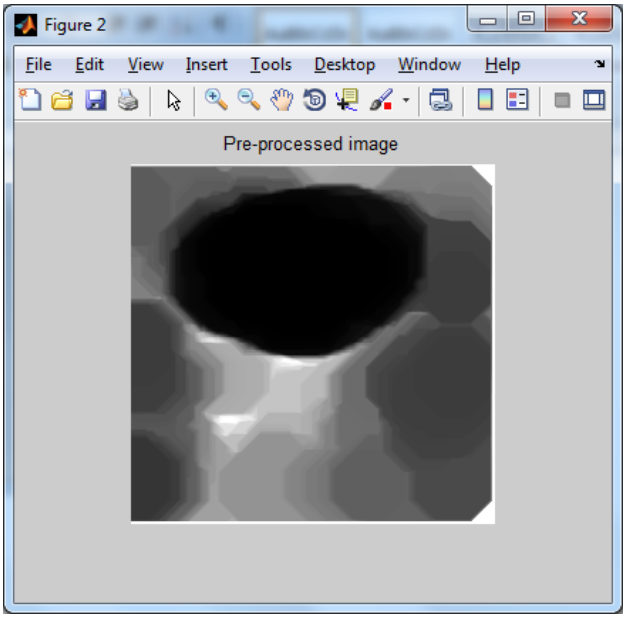

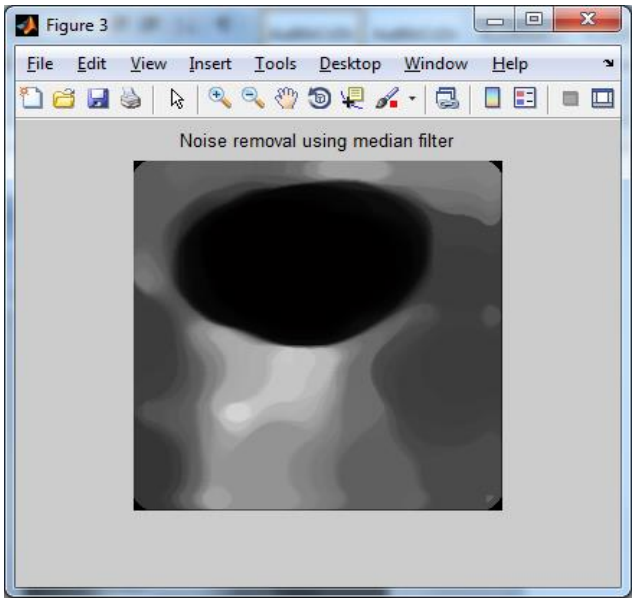

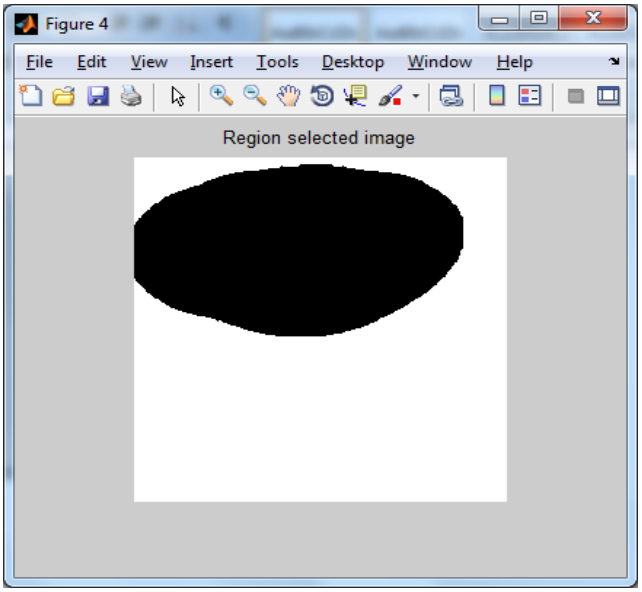

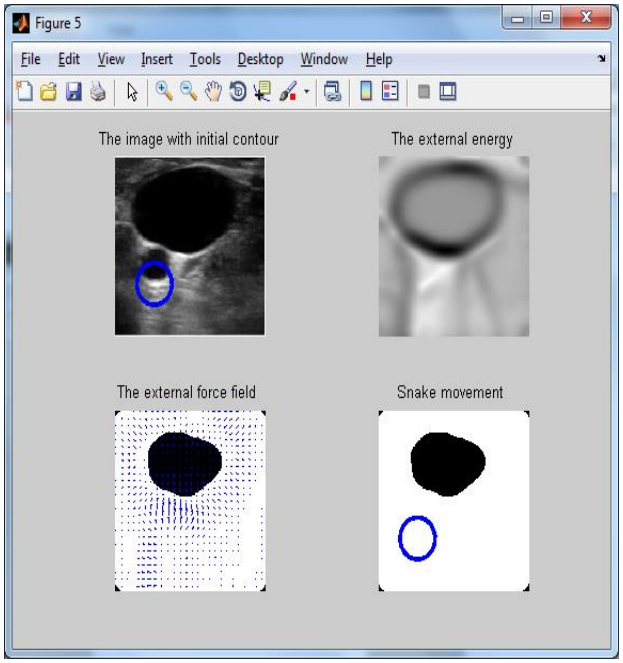

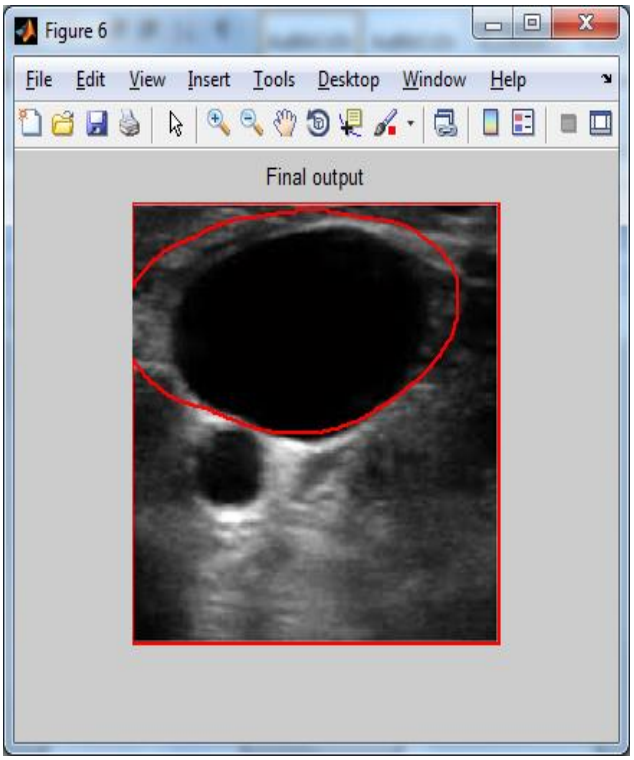

5. CONCLUSION

We were able to successfully apply a carotid segmentation method based on cervical ultrasonography. The main advantage of the novel segmentation method relies on the automatic identification of the carotid lumen, overcoming the limitations of the traditional methods. As a future work, we will test our method using more B-mode ultrasound images, including images of carotid arteries of patients with severe atherosclerosis. With the obtained contours from the segmentation of the carotid artery, 3D models will be building using algorithms of data interpolation, geometrical meshing and smoothing. With additional images acquired by computerized angiography, we expect to be able to building accurate 3D models for carotid arteries that can be posteriorly deformed and adjusted to the data obtained with the segmentation of the lumen and bifurcation structures of the carotid artery in ultrasound B-mode images. This will allow the achievement of truthful 3D models for carotid arteries from B-mode ultrasound images.

ACKNOWLEDGMENT

It is our massive pleasure to work on this project, segmentation by using Ultrasound images in medical image processing. It is only the approval of my delightful master which has prompted and mentally equipped us to undertake the study of this project. Here we would like to thank, Principal Dr.S.Suresh Kumar, Vivekanandha College of Engineering for Women for giving us such a chance to enhance practical understanding about subject. We are grateful to Dr.D.Sasikala, Head of Electronics and Communication Engineering Department for her valuable support at each part of our project work. I put forward my frank thanks to my lead Prof.Dr.D.Sasikala kindly encourages us to work on the subject and gave his helpful assistance time to time.

REFERENCES

[1] A. J. Lusis, "Atherosclerosis," *Nature,* vol. 407, pp. 233−241, 2000.

[2] D. Mozaffarian et al., "Heart disease and stroke statistics − 2015 update," *American Heart Association Statistical Update, Circulation,* vol. 131, pp. e179−e205, 2015.

[3] I. Shai et al., "Dietary intervention to reverse carotid atherosclerosis," *Epidemiology and Prevention, Circulation,* vol. 121, pp. 1200−1208, 2010.

[4] F. Mao, J. Gill, D. Downey, and A. Fenster, "Segmentation of carotid artery in ultrasound images: Method development and evaluation technique," *Medical Physics,* vol. 27, no. 8, pp. 1961−1970, 2000.

[5] A. Hamou and M. EI-Sakka, "A novel segmentation technique for carotid ultrasound images," *in Proc. IEEE Intl. Conf. on Acoustics, Speech, and Signal Processing,* pp. 521−524, 2004.

[6] A. R. Abdel-Dayem, M. El-Sakka, and A. Fenster, "Watershed segmentation for carotid artery ultrasound images*," in Proc. 3rd ACS/IEEE Intl. Conf. on Computer Systems and Applications,* pp. 131−139, 2005.

[7] A. Hamou, S. Osman, and M. El-Sakka, "Carotid ultrasound segmentation using dp active contours," *Image Analysis and Recognition, Lecture Notes in Computer Science, Springer,* vol. 4633, pp. 961−971, 2007.

[8] J. Stoitsis, S. Golemati, S. Kendros, and K.S. Nikita, "Automated detection of the carotid artery wall in b- mode ultrasound images using active contours initialized by the hough transform," *in Proc. 30th Annual Intl. Conf. of the IEEE Engineering in Medicine and Biology Society,* pp. 3146−3149, 2008.

[9] X. Yang, M. Ding, L. Lou, M. Yuchi, W. Qiu, and Y. Sun, "Common carotid artery lumen segmentation in b- mode ultrasound transverse view images," *Intl. Journal of Image, Graphics and Signal Processing,* vol. 3, no. 5, pp. 15−21, 2011.

[10] X. Yang, W. He, J. Jin, X. Zhang, M. Yuchi, and M. Ding, "A hybrid method to segment common carotid arteries from 3D ultrasound images," *in Proc. IEEE- MBS Intl. Conf on Biomedical and Health Informatics,* pp. 241−244, 2012.

[11] K. Riha, J. Masek, R. Burget, R. Benes, and E. Zavodna, "Novel method for localization of common carotid artery transverse section in ultrasound images using modified Viola-Jones detector," *Ultrasound in Medicine and Biology*, vol. 39(10). pp. 1887−1902, 2013.

[12] Artery databases, *Signal Processing Laboratory: http://www.splab.cz/en/research/zpracovani-medicinskych-signalu/databaze/artery.*

[13] X. Yang, J. Jin, M. Xu, H. Wu, W. He, M. Yuchi, and M. Ding, "Ultrasound common carotid artery segmentation based on active shape model," *Computational and Mathematical Methods in Medicine,* vol. 2013(345968), pp. 01−11, 2011.

[14] E. Ukwatta, J. Awad, A. D. Ward, D. Buchanan, G.Parraga, and A. Fenster, "Coupled level-set approach to segment carotid arteries from 3D ultrasound images," *in Proc. IEEE Intl. Symposium on Biomedical Imaging,* pp. 37−40, 2011.

[15] S. Chaudhuri, S. Chatterjee, N. Katz, M. Nelson, and M. Goldbaum, "Detection of blood vessels in retinal images using two-dimensional matched filters," *IEEE Trans. on Medical Imaging,* vol. 8, no. 3, pp. 263−269, 1989.

[16] J. R. Harish Kumar, A. K. Pediredla, and C. S. Seelamantula, "Active discs for automated optic disc segmentation," *in Proc. IEEE Global Conf. on Signal and Information Processing,* pp. 225−229, 2015.

[17] A. K. Pediredla and C. S. Seelamantula, "A unified approach for optimization of snakuscules and ovuscules," *in Proc. IEEE Intl. Conf. on Acoustics, Speech, and Signal Processing,* pp. 681−684, 2012.

[18] P. Thévenaz, and M. Unser, "Snakuscules," *IEEE Trans. on Image Processing,* vol. 17, no. 4, pp. 585−593, 2008.

[19] E. K. P. Chong and S. H. Zak, An Introduction to Optimization. *Wiley-lnderscience, Second Ed.,* pp. 115−134, 2001.

[20] G. F. Simmons, Calculus with Analytic Geometry. *The McGraw-Hill Companies, Inc., Second Ed.,* pp. 764−770, 1996.

[21] W. R. Crum, O. Camara, and D. L. G. Hillu, "Generalized overlap measures for evaluation and validation in medical image analysis," *IEEE Trans. on Medical Imaging,* vol. 25, no. 11, pp. 1451−1461, 2006.

[22] W. K. Pratt, Introduction to Digital Image Processing, *CRC Press,* pp. 595−599, 2014.

[23] *Image J: http://www.imagej.nih.gov/ij.*

[24] K. Riha, P. Chen, and D. Fu, "Detection of artery section area using artificial immune system algorithm," *in Proc. of the 7th WSEAS Intl. Conf. on Circuits, Systems, Electronics, Control, and Signal Processing,* pp. 46−52, 2008.